Introduction to Large Eddy Simulation of Turbulent Flows [1]

J. Fröhlich, W. Rodi

Institute for Hydromechanics, University of Karlsruhe,
Kaiserstraße 12, D-76128 Karlsruhe, Germany

Contents

[1] appeared in: B.E. Launder, N.D. Sandham (eds.), Closure Strategies for Turbulent and Transitional Flows, Cambridge University Press, Chapter 8, p.267–298, 2002

1 Introduction

This chapter is meant as an introduction to Large–Eddy Simulation (LES) for readers not familiar with it. It therefore presents some classical material in a concise way and supplements it with pointers to recent trends and literature. For the same reason we shall focus on issues of methodology rather than applications. The latter are covered elsewhere in this volume. Furthermore, LES is closely related to direct numerical simulation (DNS) which is also discussed in several chapters of this volume. Hence, we concentrate as much as possible on those features which are particular to LES and which distinguish it from other computational methods.

For the present text we have assembled material from research papers, earlier introductions and reviews (Ferziger(1996), Härtel (1996), Piomelli (1998)), and our own results. The selection and presentation is of course biased by the authors' own point of view. Supplementary material is available in the cited references.

1.1 Resolution requirements of DNS

The principal difficulty of computing and modelling turbulent flows resides in the dominance of non–linear effects and the continuous and wide spectrum of observed scales. Without going into details (the reader might consult classical text books such as Tennekes & Lumley (1972)) we just recall here that the ratio of the size of the largest turbulent eddies in a flow, L, to that of the smallest ones determined by viscosity, η, behaves like $L/\eta \sim Re_{u'}^{3/4}$. Here, $Re_{u'} = u'\,L/\nu$ with u' being a characteristic velocity fluctuation and ν the kinematic viscosity. Let us consider as an example a plane channel, a prototype of an internal flow. Reynolds (1989) estimated $Re_{u'} \sim Re^{0.9}$ from $u' \sim u\,c_f^{1/2}$, $c_f \sim Re^{-0.2}$, where Re is based on the center line velocity and the channel height. In a DNS no turbulence model is applied so that motions of all size have to be resolved numerically by a grid which is sufficiently fine. Hence, the computational requirements increase rapidly with Re. According to this estimate a DNS of channel flow at $Re = 10^6$ for example would take around hundred years on a computer running at several GFLOPS. This is obviously not feasible. Moreover, in an expensive DNS a huge amount of information would be generated which is mostly not required by the practical user. He or she would mostly be content with knowing the average flow and some lower moments to a precision of a few percent. Hence, for many applications a DNS which is of great value for theoretical investigations and model testing is not only unaffordable but would also result in computational overkill.

1.2 The basic idea of LES

Suppose somebody wants to perform a DNS but the grid that would be required exceeds the capacity of the available computer; so a coarser grid is used. This coarser grid is able to resolve the larger eddies in the flow but not the ones which are smaller than one or two cells. From a physical point of view, however, there is an interaction between the motions on all scales so that the result for the large scales would generally be wrong without taking into account the influence of the fine scales on the large ones. This requires a so–called subgrid–scale model as discussed below. Hence, LES can be viewed as a 'poor man's DNS'. The poor man, however, has to compensate by cleverness in that a model for the unresolved motion has to be devised and an intricate coupling between physical and

numerical modelling is generated. On the other hand, the resolution of the large scales of the flow while modelling only the small ones – not the entire spectrum – is an advantage of the LES approach compared to methods based on the Reynolds averaged Navier–Stokes equations (RANS). The latter methods often have difficulties when applied to complex flows with pronounced vortex shedding or special influences of buoyancy, curvature, rotation or compression. Finally, LES gives access to the dominant unsteady motion so that it can, for example, be used to study aero–acoustics, fluid–structure coupling or the control of turbulence by an appropriate unsteady forcing.

2 Governing equations and Filtering

The Navier–Stokes equations (NSE) constitute the starting point for any turbulence simulation. Here, we consider incompressible, constant–density fluids for which these equations read

$$\frac{\partial u_i}{\partial x_i} = 0 \tag{1}$$

$$\frac{\partial u_i}{\partial t} + \frac{\partial \left(u_i u_j\right)}{\partial x_j} + \frac{\partial \Pi}{\partial x_i} = \frac{\partial(\nu\, 2S_{ij})}{\partial x_j} \tag{2}$$

where $S_{ij} = (\partial u_j/\partial x_i + \partial u_i/\partial x_j)/2$ is the strain–rate tensor and $\Pi = p/\rho$. For later reference we introduce Reynolds averaging which is used in statistical turbulence modelling (RANS) as time averaging: $\langle u \rangle = \lim_{T\to\infty} \frac{1}{T} \int_0^T u\ dt$. Reynolds averaging has the properties

$$\langle\langle u \rangle\rangle \;=\; \langle u \rangle, \quad \langle u \langle v \rangle\rangle \;=\; \langle u \rangle \langle v \rangle. \tag{3}$$

According to the idea of LES a means is required to distinguish between small, unresolved, and larger, resolved structures. This is accomplished by the operation $u \mapsto \overline{u}$ defined below. Unlike the above Reynolds time averaging it is an operation in space. The fact that RANS and LES methods employ averaging in different dimensions inhibits an easy link between them. Several attempts have been made to put both in a common framework (Speziale 1998, Germano 1999) but will not be discussed here. We now turn to the ways of defining $\overline{u}$ and illustrate them in the one–dimensional case.

2.1 Schumann's approach

The 'volume–balance approach' of Schumann (1975) starts from a given finite volume mesh. The integral of a continuous unknown $u(x)$ in (1),(2) over one cell is denoted ${}^V\overline{u} = \frac{1}{\Delta x}\int_V u(x)dx$ as illustrated in Fig. 1 (indices referring to cells are dropped). Integrating the NSE over a cell and using Gauss' theorem relates these values to surface–averaged quantities denoted ${}^j\overline{\cdots}$, such as ${}^j\overline{uv}$. These need to be expressed in terms of the cell–averages, which is done in two steps. If the discretization is sufficiently fine replacing ${}^j\overline{uv}$ by ${}^j\overline{u}{}^j\overline{v}$ as is usual in finite volume methods is possible with only a minor approximation error. This is done in DNS. If the grid is not fine enough, however,the difference can be significant and the unresolved momentum flux ${}^j\overline{uv} - {}^j\overline{u}{}^j\overline{v}$ has to be accounted for by a model, the so–called subgrid–scale (SGS) model. Subsequently, ${}^j\overline{u}$ are related to the ${}^V\overline{u}$ either by setting them equal to cell averaged quantities if a staggered arrangement is used

or by interpolating from neighbouring values. The final SGS contribution to be modelled therefore also depends on the expressions used for ${}^{j}\overline{u}$, i.e. on the discretization scheme. To sum up, the equations are discretized and with discretizing them the splitting into large and small scales is performed since the latter cannot be resolved by the discrete system. Observe that the operations $u \mapsto {}^{V}\overline{u}$ and $u \mapsto {}^{j}\overline{u}$ map an integrable function onto discrete values, a continuous function $\overline{u}(x)$ is not constructed. Thus, with Schumann's approach, scale separation, discretization, and SGS model are not separated conceptually but intimately tied together. This has advantages in that anisotropies and inhomogeneities of the grid can easily be incorporated. However, it renders the analysis of the various contributions to the solution relatively difficult and hence is considered too restrictive by many workers in the field.

2.2 Filtering

Leonard (1974) proposed to define $\overline{u}$ by

$$\overline{u}(x) = \int_{-\infty}^{+\infty} G\,(x - x')\;\; u\,(x')\;\; dx' \quad . \tag{4}$$

An integral of this kind is called a convolution. Here, G is a compactly supported or at least rapidly decaying filter function with $\int G(x)\; dx = 1$ and width $\overline{\Delta}$. The latter can be defined by the second moment of G as $\overline{\Delta} = \sqrt{12 \int x^2 G(x)\; dx}$. Fig. 2 displays the Gaussian Filter $G_G = \sqrt{6/\pi}\;\, 1/\overline{\Delta}\;\, \exp(-6x^2/\overline{\Delta}^2)$ and the box filter defined by $G_B = 1/\overline{\Delta}$ if $|x| \leq \overline{\Delta}/2$ and $G_B = 0$ elsewhere. In fact, already Deardorff (1966) used (4) in the special case $G = G_B$. Figs. 3a and 3b illustrate the filtering with smaller or larger filter width: the larger $\overline{\Delta}$, the smoother is $\overline{u}$. According to (4) $\overline{u}$ is a continuous smooth function as displayed in Fig. 3 which can subsequently be discretized by any numerical method. This has the advantage that one can separate conceptually the filtering from the discretization issue.

It is helpful to transfer eq. (4) to Fourier space by means of the definition $\hat{u}(\omega) = \int u(x)\; e^{-i\omega x}\; dx$, since in Fourier space, where the spatial frequency ω is the independent variable, a convolution integral turns into a simple product. Eq. (4) then reads

$$\widehat{\overline{u}}(\omega) = \widehat{G}(\omega)\, \widehat{u}(\omega) \quad . \tag{5}$$

Figure 4 illustrates the filtering in Fourier space. Equation (5) allows the definition of another filter, the Fourier cutoff filter with $\widehat{G}_F(\omega) = 1$ if $|\omega| \leq \pi/\overline{\Delta}$ and 0 elsewhere. From (5) it is obvious that only this filter yields $\overline{\overline{u}} = \overline{u}$ since $(\widehat{G}_F)^2 = \widehat{G}_F$. In all other cases the identity is not fulfilled. This can be appreciated by comparing $\overline{\overline{u}}$ and $\overline{u}$ for the box filter in Figs. 3 and 4. The second relation in (3) is never fulfilled except in trivial cases, so that for general filtering we have

$$\overline{\overline{u}} \neq \overline{u}, \quad \overline{u\overline{v}} \neq \overline{u}\;\overline{v} \tag{6}$$

which distinguishes clearly the filtering in LES from Reynolds averaging (see Germano (1992) for a detailed discussion). The vertical line in Fig. 4 represents the nominal cutoff at $\pi/\overline{\Delta}$ related to the grid. The Fourier cutoff filter $\widehat{G_F}$ would yield a spectrum of $\overline{u}$ which is equal to the one of u left of this line and zero right of it. Eq. (5) and Fig. 4 therefore demonstrate that when a general filter is applied, such as the box filter, this does not yield a neat cut through the energy spectrum but rather some smoother decay to zero. This is

important since SGS modelling often assumes that the spectrum of the resolved scales near the cutoff follows an inertial spectrum with a particular slope and a particular amount of energy transported from the coarse to the fine scales on the average. We see that even if u fulfills this property this can be altered by the filtering (for further remarks see Section 4.3). Nevertheless, it is convenient and common to use the notion of a simple cutoff as a model in qualitative discussions. Eq. (5) is also helpful to illustrate that derivative and filter commute, i.e. $\partial\overline{u}/\partial x = \overline{(\partial u/\partial x)}$. Any convolution filter (4) can be written as in (5) regardless of the choice of G. Differentiation appears as multiplication by $i\omega$ in Fourier space, eq. (28) below, which is commutative.

Applying the three–dimensional equivalent of the filter (4) to the NSE (1) and (2), the following equations for the filtered velocity components $\overline{u_i}$ result

$$\frac{\partial \overline{u}_i}{\partial x_i} = 0 \tag{7}$$

$$\frac{\partial \overline{u_i}}{\partial t} + \frac{\partial\left(\overline{u_i}\,\overline{u_j}\right)}{\partial x_j} + \frac{\partial \overline{\Pi}}{\partial x_i} = \frac{\partial(\nu\, 2\overline{S}_{ij})}{\partial x_j} - \frac{\partial \tau_{ij}}{\partial x_j} \tag{8}$$

where $\overline{S}_{ij}$ and $\overline{\Pi}$ are defined analogous to the unfiltered case. The term

$$\tau_{ij} \;=\; \overline{u_i u_j} - \overline{u}_i \overline{u}_j \tag{9}$$

represents the impact of the unresolved velocity components on the resolved ones and has to be modelled. In mathematical terms it arises from the nonlinearity of the convection term which does not commute with the linear filtering operation.

An important property of $\overline{u_i}$ is that it depends on time. Hence, an LES necessarily is an unsteady computation. Furthermore, $\overline{u_i}$ always depends on all three space–dimensions (except for very special cases). Symmetries of the boundary conditions generally produce the same symmetries for the RANS variable $\langle u_i \rangle$, e.g. vanishing dependence on a homogeneous direction. However, due to the very nature of turbulence this does not hold for $\overline{u_i}$ since the instantaneous turbulent motion is always three–dimensional. The fact that a three–dimensional unsteady flow is to be computed makes LES a computationally demanding approach. We finally note that for any filter the term in (9) vanishes in the limit $\overline{\Delta} \to 0$, since then $\overline{u} \to u$ according to (4), and all scales are resolved so that the LES turns into a DNS.

2.3 Variable filter size

It should be mentioned here that filtering as defined by (4) is not easily compatible with boundary conditions. Applying a box filter of constant size $\overline{\Delta}$ for instance yields $\overline{u} \neq 0$ within a distance $\overline{\Delta}/2$ outside of the computational domain and raises the question of how to impose boundary conditions for $\overline{u}$. This issue is removed by supposing G to be x–dependent and locally asymmetric. However, if $G(x-x')$ is generalized to some $G(x,x')$ or if the prolongation of u from a finite domain to the real axis induces discontinuities, the commutation property is lost and additional commutator terms arise in (7), (8) (Ghosal & Moin 1995). In contrast to the usual SGS term τ_{ij}, which is generated by the nonlinearity of the convection term, the commutator also appears for linear expressions (see the discussion by Geurts (1999) and Section 4.3). This issue is relevant for pronounced grid stretching in the interiour of the domain and close to walls but has been disregarded until recently. Studies for a channel flow are reported in (Fröhlich et al. 1998, 2000).

2.4 Implicit versus explicit filtering

The filtering approach relaxes the link between the size of the computed scales and the size of the grid since the filter can be coarser than the employed grid. Consequently, the modelled motion should be called subfilter– rather than subgrid–scale motion. The latter labelling results from the Schumann–type approach and is frequently used for historical reasons to designate the former. In practice, however, the filter G does not appear explicitly at all in many LES codes [2] so that in fact the Schumann approach is followed. Due to the conceptual advantages of the filtering approach reconciliation of both is generally attempted in two ways. The first observation is that a finite difference method for (7), (8) with a box filter employs the same discrete unknowns as Schumann's approach, such as $\overline{u}(x_k) = {}^{V_k}\overline{u}$ with k referring to a grid point. Choosing appropriate finite difference formulae the same or very similar discretization matrices are obtained in both cases. Another argument is that the definition of discrete unknowns amounts to an 'implicit filtering' – i.e. filtering with some unknown filter (but one that in principle exists) – since any scale smaller than the grid is automatically discarded. In this way the filter is more or less used symbolically only to make the effect of a later discretization appear in the continuous equations. This is easier in terms of notation and stimulates physical reasoning for the subsequent SGS modelling.

In contrast to implicit filtering one can use a computational grid finer than the width of G and only retain the largest scales by some (explicit) filtering operation. This explicit filtering is recently being advocated by several authors such as Moin (1997) since it considerably reduces numerical discretization errors as the retained motion is always well resolved. On the other hand it increases the modelling demands since for the same number of grid points more scales of turbulent motion have to be modelled and it is up to now not fully clear which approach is more advantageous (Lund & Kaltenbach 1995). The filtering approach of Leonard is almost exclusively introduced today in papers on LES and has triggered substantial development, e.g. in subgrid–scale modelling. In practice, however, it is most often used rather as a concept than as a precise algorithmic construction.

3 Subgrid–scale modelling

3.1 Introduction

Subgrid-scale modelling is a particular feature of LES and distinguishes it from all other approaches. It is well–known that in three–dimensional turbulent flows energy cascades in the mean from large to small scales. The primary task of the SGS model therefore is to ensure that the energy drain in the LES is the same as obtained with the cascade fully resolved as in a DNS. The cascading, however, is an average process. Locally and instantaneously the transfer of energy can be much larger or much smaller than the average and can also occur in the opposite direction ("backscatter") (Piomelli et al. 1996). Hence, ideally, the SGS model should also account for this local, instantaneous transfer. If the grid scale is much finer than the dominant scales of the flow, even a crude model will suffice to yield the right behaviour of the dominant scales. This is due to two reasons. First, the larger the distance in wavenumber space between different contributions the looser is

[2] Apart from some filtering operations for the dynamic model, discussed below, which is of a somewhat different nature

their coupling. Second, as a consequence of this as well as of the energy cascading, the finer scales exhibit a more universal character which is more amenable to modelling. On the other hand, if the grid scale is coarse and close to the most energetic, anisotropic, and inhomogeneous scales the SGS model should be of better quality. Obviously, there exist two possible approaches, one is to improve the SGS model and the other is to refine the grid. In the limit, the SGS contribution vanishes and the LES turns into a DNS. Refining the grid, however is restricted due to the rapid increase of the computational cost. The alternative strategy, for example solving an additional transport equation in a more elaborate SGS model, can be comparatively inexpensive.

Another aspect results from the numerical discretization scheme which introduces a difference between the continuous differential operators and their discrete equivalents. This difference is particularly large close to the cutoff scale. For DNS this is not so disturbing, but with LES precisely these scales have a substantial influence on the modelled SGS contribution as will be illustrated below. Hence, in LES the discretization scheme and the SGS model have to be viewed together. Indeed, some schemes such as low order upwind discretizations generate a considerable amount of numerical dissipation as discussed in Section 5.2 below. Therefore certain authors perform LES without any explicit SGS model (Tamura, Ohta & Kuwahara 1990, Meinke et al. 1998). The grid is refined as much as possible to decrease the importance of the SGS terms, and the energy drain is in one way or another accomplished by the numerical scheme. Although yielding valuable results in some cases, this kind of modelling can hardly be evaluated or controlled. Hence, in most LES central or spectral schemes are used and the SGS term is represented by an explicit model.

We shall now turn to the description of some basic SGS models before giving a summarizing view at the end of this section.

3.2 Smagorinsky model

The Smagorinsky model (SM) (Smagorinsky 1963) was the first SGS model and is still widely used. As with most of the current SGS models, it employs the concept of an eddy viscosity, relating the traceless part of the SGS stresses, τ_{ij}^a, to the strain rate $\overline{S_{ij}}$ of the resolved velocity field:

$$\tau_{ij}^a = \tau_{ij} - \frac{1}{3}\delta_{ij}\tau_{kk} = -2\nu_t \overline{S}_{ij} \tag{10}$$

The advantage of (10) is that the resulting equation for $\overline{u_i}$ to be solved looks like (2) with $\overline{u_i}$ instead of u_i, $\overline{\Pi} + \frac{1}{3}\delta_{ij}\tau_{kk}$ instead of Π, and $\nu + \nu_t$ instead of ν. Hence, it is very easy to incorporate this into an existing solver for the unsteady NSE.

The second part of this model is the determination of the eddy viscosity ν_t. Dimensional analysis yields

$$\nu_t \propto l\, q_{SGS} \tag{11}$$

where l is the length scale of the unresolved motion and q_{SGS} its velocity scale. From the above discussion it is natural to use the filter size $\overline{\Delta}$ as the length scale, hence setting $l = C_s\overline{\Delta}$. Similar to Prandtl's mixing length model, the velocity scale is related to the gradients of $\overline{u_i}$ expressed by

$$q_{SGS} \;=\; l\,|\overline{S}| \qquad |\overline{S}| = \sqrt{2\overline{S}_{ij}\overline{S}_{ij}} \tag{12}$$

which yields

$$\nu_t = (C_s\overline{\Delta})^2|\overline{S}| \tag{13}$$

This amounts to assuming local equilibrium between the production of the SGS kinetic energy, $P = -\tau_{ij}^a\ \overline{S}_{ij}$ and dissipation ε expressed by q_{SGS}^3/l. Introducing (10) and (12) in $P = \epsilon$ gives (13). The constant C_s can be determined assuming an inertial–range Kolmogorov spectrum for isotropic turbulence which yields $C_s = 0.18$. This value has turned out to be too large for most flows so that often $C_s = 0.1$ or even lower values are used. Close to walls ν_t has to be reduced to account for the anisotropy of the turbulence. This is generally accomplished by replacing C_s in (13) with $C_sD(y^+)$. Most often the van Driest damping

$$D(y^+) = 1 - e^{-y^+/A^+} \quad , \quad A^+ = 25 \tag{14}$$

is used which is known from statistical models. However, this yields $\nu_t \sim (y^+)^2$ for small y^+ while ν_t should behave like y^{+3}. The correct behaviour is achieved by the alternative damping function (Piomelli, Moin & Ferziger 1993)

$$D(y^+) = \left(1 - e^{-(y^+/A^+)^3}\right)^{1/2} \tag{15}$$

The main reason for the frequent use of the SM is its simplicity. Its drawbacks are that the parameter C_s has to be calibrated and its optimal value may vary with the type of flow, the Reynolds number, or the discretization scheme. The kind of damping to be applied near a wall is a further point of uncertainty. Also, the SM, like any other model based on (10) with $\nu_t \geq 0$, is strictly dissipative and does not allow for backscatter. It is furthermore not appropriate for simulating transition since it yields $\nu_t \geq 0$ even in laminar flows.

3.3 Dynamic procedure

From the previous section it is apparent that for physical reasons one would prefer to replace the constant value C_s by a value changing in space and time. The dynamic procedure has been developed by Germano et al. (1991) in order to determine such a value from the information provided by the resolved scales, in particular the ones close to the cutoff scale. In fact this procedure can be applied with any model $\tau_{ij}^{mod}(C, \Delta, u)$ for τ_{ij} or τ_{ij}^a containing a parameter C. [3] The basic idea is to employ the model chosen not only on the grid scale, or filter scale, $\overline{\Delta}$ but also on a coarser scale $\widehat{\Delta}$ as illustrated in Fig. 5. This is the so–called test scale with, e.g., $\widehat{\Delta} = 2\overline{\Delta}$:

$$\text{sub–grid scale stresses } (\overline{\Delta}\text{–level}) \ : \quad \tau_{ij} = \overline{u_iu_j} - \overline{u_i}\,\overline{u_j} \quad \approx \quad \tau_{ij}^{mod}(C, \overline{\Delta}, \overline{u}) \tag{16}$$

$$\text{sub–test scale stresses } (\widehat{\Delta}\text{–level}) \ : \quad T_{ij} = \widehat{\overline{u_iu_j}} - \widehat{\overline{u_i}}\,\widehat{\overline{u_j}} \quad \approx \quad \tau_{ij}^{mod}(C, \widehat{\Delta}, \widehat{\overline{u}}) \tag{17}$$

From the known resolved velocities $\overline{u_i}$ the velocities $\widehat{\overline{u_i}}$ can be computed by applying the filter $\widehat{..}$ to $\overline{u_i}$ using an appropriate function $\widehat{G}$. Similarly, the term $L_{ij} = \widehat{\overline{u_i}\,\overline{u_j}} - \widehat{\overline{u_i}}\,\widehat{\overline{u_j}}$ can be evaluated. It is this part of the sub–test stresses T_{ij} which is resolved on the grid $\overline{\Delta}$ as sketched in Fig. 5 : The total stresses $\overline{u_iu_j}$ in the expression for T_{ij} can be decomposed

[3] In this subsection we distinguish between exact and modelled SGS stresses for clarity.

into the contribution $\overline{u_i}\,\overline{u_j}$ resolved on the grid $\overline{\Delta}$ and the remainder τ_{ij}. Inserting this in (17) gives

$$T_{ij} = L_{ij} + \widehat{\tau_{ij}} \tag{18}$$

known as Germano's identity. Hence, on one hand L_{ij} can be computed, on the other hand the SGS model yields a model expression when inserting (16),(17) in (18) :

$$L_{ij}^{mod} = \tau_{ij}^{mod}(C, \widehat{\Delta}, \widehat{\overline{u}}) - \widehat{\tau_{ij}^{mod}(C, \overline{\Delta}, \overline{u})} \tag{19}$$

Ideally, C would be chosen to yield

$$L_{ij} - L_{ij}^{mod} = 0 \tag{20}$$

but this is a tensor equation and can only be fulfilled in some average sense, minimizing e.g. the root mean square of the left hand side as proposed by Lilly (1991). Principally, the consecutive application of $\widehat{G}$ and $\overline{G}$ to obtain $\widehat{\overline{u}}$ yields an effective filter, of width $\widehat{\overline{\Delta}} \neq \widehat{\Delta}$, which generally is even of different type as $\widehat{G}$ and $\overline{G}$ (e.g. when the box filter is used). This issue is generally neglected in the literature. For that reason and since $\widehat{\overline{\Delta}} = \widehat{\Delta}$ with the Fourier cutoff filter presently used for illustration we write $\widehat{\Delta}$ instead of $\widehat{\overline{\Delta}}$ in this section. Effectively, it is the ratio $\widehat{\overline{\Delta}}/\overline{\Delta}$ which is required by the dynamic models.

We now apply the dynamic procedure to the SM (10),(13) and get

$$L_{ij}^{mod} = -2\,C\,\widehat{\Delta}^2|\widehat{\overline{S}}|\widehat{\overline{S}}_{ij} + \widehat{2\,C\,\overline{\Delta}^2|\overline{S}|\overline{S}_{ij}} \tag{21}$$

with $C = C_s^2$ for convenience. Classically, the model is developed by extracting C from the filtered expression in the second term although in fact C will vary in space. The right hand side of (21) can then be written as $-2CM_{ij}$ so that inserting into (20) with the least–squares minimization mentioned above yields

$$C = -\frac{1}{2}\frac{L_{ij}\,M_{ij}}{M_{ij}\,M_{ij}} \tag{22}$$

The advantage of (22) or a similar equation is that now the parameter of the SM is no longer required from the user but is determined by the model itself. In fact, it is automatically reduced close to walls and vanishes for well–resolved laminar flows. Negative values of C are possible and can be viewed as a way to model backscatter. The resulting "backward diffusion" can however generate numerical instability so that often $\nu + \nu_t \geq 0$ is imposed. Furthermore, C determined by (22) as it is, exhibits very large oscillations which generally need to be regularized in some way. Most often L_{ij} and M_{ij} are averaged in spatially homogeneous directions space before being used in (22). However, this requires the flow to have at least one homogeneous direction. Another way is to relax the value in time according to $C^{n+1} = \epsilon C + (1-\epsilon)C^n$ using C^n from the previous time step (Breuer & Rodi 1994). Yet another way is to use the known value C^n in the rightmost term of (21) so that it need not be extracted from the test filter (Piomelli & Liu 1995). This yields smoothing in space without any homogeneous direction required.

3.4 Scale similarity models

Scale similarity models (SSM) have been created to overcome the drawbacks of eddy viscosity–type models. Filtering the decomposition $u_i = \overline{u}_i + u_i'$ yields the (exact) relation

$$\overline{u_i'} = \overline{u_i} - \overline{\overline{u_i}}. \tag{23}$$

This can be interpreted as equality between the largest contributions of u_i' and the smallest contributions of $\overline{u_i}$ (see Fig. 4). Furthermore, it is computable from $\overline{u_i}$. Introducing the decomposition of u_i into (9) and modelling $\overline{u_i'u_j'} \approx \overline{u_i'}\ \overline{u_j'}$ and $\overline{u_i'\overline{u_j}} \approx \overline{u_i'}\ \overline{\overline{u_j}}$, respectively, yields the model $\tau_{ij}^a = L_{ij}^{m,a}$ with

$$L_{ij}^m = \overline{\overline{u_i}\ \overline{u_j}} - \overline{\overline{u_i}}\ \overline{\overline{u_j}} \tag{24}$$

and $...^a$ indicating the traceless part of a tensor. For a spectral cutoff filter $\overline{\overline{u}}$ is replaced by $\widehat{\overline{u}}$ with $\widehat{\Delta} = \sqrt{2}\,\Delta$ since for this filter $\overline{\overline{u}} = \overline{u}$ as discussed above.

The SSM allows backscatter, i.e. transfer of energy from fine to coarse scales, and does not impose alignment between the SGS stress tensor τ_{ij} and the strain rate $\overline{S}_{ij}$. On the other hand, (24) turns out to be not dissipative enough so that it is generally combined with a Smagorinsky model. Horiuti (1997) subsumes some current SSMs in the model

$$\tau_{ij}^a = C_L L_{ij}^{m,a} + C_B L_{ij}^{R,a} - 2C_\nu \overline{\Delta}^2 \mid \overline{S} \mid \overline{S}_{ij} \tag{25}$$

with $L_{ij}^R = \overline{\overline{u_i'}\ \overline{u_j'}} - \overline{\overline{u_i'}}\ \overline{\overline{u_j'}}$, evaluated using (23). A further step is to combine (25) with the dynamic procedure for the determination of the constants: (a) C_ν with $C_L = 1, C_B = 0$ (Zang, Street & Koseff 1993) (b) C_L and C_ν with $C_B = 0$ (Salvetti & Banerjee 1995) (c) C_B and C_ν with $C_L = 1$ (Horiuti 1997). Different tests in the cited references as well as by Piomelli, Yu & Adrian (1996) show that SSMs in conjunction with the dynamic procedure perform quite well for low order finite difference or finite volume methods. Apart from the ability to represent backscatter this may also be due to the fact that no spatial derivatives are involved in the SSM which reduces the impact of numerical discretization errors.

3.5 Further models and comparative discussion

Let us sum up a few strategies or concepts which are currently followed in SGS modelling. One, already mentioned in the beginning of this section, is to employ a crude model and to compensate by grid refinement which decreases the impact of the model.

Another strategy is to employ the same approaches as in RANS modelling. The Smagorinsky model based on an eddy–viscosity and an algebraic mixing–length expression is the most prominent example. But as with RANS, more elaborate methods can be used to compute the turbulent viscosity such as a model employing a transport equation for the SGS kinetic energy $k_{SGS} = 1/2\tau_{kk}$ which furnishes a velocity scale $q_{SGS} = {k_{SGS}}^{1/2}$ (Schumann 1975, Davidson 1997). Obviously, the filter width $\overline{\Delta}$ constitutes an adequate reference length so that according to (11) $\nu_t = C\,\overline{\Delta} k_{SGS}^{1/2}$ is a reasonable model and no second length–scale determining transport equation is required. Spalart et al. (1997) have developed an approach called Detached Eddy Simulation (DES). They start from a one–equation RANS turbulence model (Spalart & Allmaras 1994) based on a transport equation for ν_t. In this equation the distance from the wall is introduced as a length scale in the destruction

term. Replacing this physical length scale by a resolution–based scale $C_D\overline{\Delta}$ (where C_D is a parameter) turns the model into a SGS model. This method furthermore offers a particular way of wall modelling which is discussed below. Still more complex approaches have been carried over from RANS. Fureby et al. (1997) employ the SGS equivalent of a Reynolds–stress model and obtain satisfactory results in some tests. The cost increase is claimed to be moderate as solving the pressure equation requires most of the work.

A third strategy, applied with SSM and the dynamic procedure, is based on the multiscale nature of turbulence. It could only be developed with scale separation defined independently from the discretization according to (4) since filtering is used as an individual operation. By analyzing experimental flow fields along these lines Liu, Meneveau & Katz (1994) propose

$$\tau_{ij} = C_L L_{ij} \tag{26}$$

with L_{ij} defined in (18). This differs from (24) since two filters of different size are used.

A fourth strategy is to relate SGS models to classical theories of turbulence. An elementary example is the determination of the Smagorinsky constant assuming a Kolmogorov spectrum. This strategy is also pursued when defining a wave–number dependent eddy viscosity to be employed with a spectral Fourier discretization and using EDQNM theory to determine $\nu_t(k)$ (Chollet & Lesieur 1981). The spectral eddy viscosity model has also been reformulated in physical space for application in complex flows yielding the structure function model (Métais & Lesieur 1992)

$$\nu_t = 0.063\overline{\Delta}\sqrt{\overline{F_2}(\overline{\Delta})} \qquad , \qquad \overline{F_2}(r) = \left(\overline{u_i}(x+r) - \overline{u_i}(x)\right)^2 \tag{27}$$

with $\overline{F_2}$ spatially averaged in an appropriate way. Different variants have been developed (Lesieur & Métais 1996). It can be shown that when implemented in a Finite Difference context, this yields a Smagorinsky–type model with $|\overline{S}|$ in (13) replaced by $|\partial\overline{u}_i/\partial x_j|$.

The last strategy we mention concerns the testing of SGS models. Of course, as with other turbulence models, prototype flows can be computed and the results then compared with experimental data or DNS results. This is still the ultimate test to pass. However, another kind of testing particular to LES has been developed, namely the so–called *a priori* test: a fully resolved velocity field from a DNS is used to explicitly compute the terms which have to be modelled in an LES on a coarser grid. The large–scale velocity on that grid is extracted to determine the SGS stresses by means of a SGS model. The difference between exact and modelled stresses reflects the quality of the model. This information should however be taken with some caution as the test involves discretization effects in a substantially different way than in the actual LES.

Finally, one has to bear in mind that a perfect SGS model is impossible. Assume the exact grid–scale velocity $\overline{u}$ being known at all points. The perfect SGS model would then amount to inferring from $\overline{u}$ on the exact instantaneous SGS velocity u' to deduce the exact instantaneous SGS stresses at all points. Since, however, infinitely many velocity fields u' are compatible with the same $\overline{u}$, even the best SGS model cannot decide which of them is realized in the actual DNS. In fact, the error introduced by missing SGS information propagates in an inverse cascade to larger scales (Lesieur 1997).

4 Numerical methods

4.1 Discretization schemes in space and time

With the filtering approach discussed in Section 2, physical modelling and numerical discretization are conceptually independent. Hence any available numerical method can in principle be used to discretize the filtered equations. A minimal requirement for precision and cost–effectiveness is that the discretization scheme is at least of second order in space and time. Classically, spectral methods were frequently used for LES and are still employed for problems with simple geometry. Derivatives are discretized most accurately and filtering and defiltering as discussed below is naturally applied in this framework. For more complex boundary conditions, finite–difference or finite–volume methods are prefered. Here, one current trend goes to unstructured meshes, another to grids with special local treatment at the boundary if this has an irregular shape.

Some numerical methods favour particular modelling ideas such as spectral methods which allow to use a spectral eddy viscosity (Chollet & Lesieur 1991) and explicit filtering by means of (5). Others need particular care in certain points. For example if implicit filtering is used together with a type of finite element that has a different number of degrees of freedom for velocity compared to pressure (which is classically the case for stability reasons), this results in a different amount of filtering for these quantities and can deteriorate the result (Rollet–Miet, Laurence & Ferziger 1999). Discretizations in space can be selected according to relevant properties such as ability to treat complex geometries, cost per grid point, etc. If possible, however, equispaced grids are used since the influence of grid–inhomogeneity and grid–anisotropy on SGS modelling is not yet fully mastered. A comparative study of a structured and an unstructured method for the same problem was undertaken by Fröhlich et al. (1998) where, for the particular case considered, adaptivity of the former method was roughly compensated by higher cost per node. For more complex geometries unstructured methods are certainly favourable.

Concerning the time scheme we already noted that temporal resolution has to be compatible with resolution in space so that $C = \overline{u}\,\Delta t/\Delta x \leq O(1)$. Since this type of limit is equivalent to the stability limit of explicit methods, in many cases the latter are typically used for LES. Adams–Bashforth, Runge–Kutta or leap–frog schemes are the most popular ones. If the diffusion limit is stricter in a computation, semi–implicit time stepping can be more efficient.

4.2 Analysis of numerical schemes for LES

The essential feature that distinguishes LES from DNS is that the smallest resolved grid–scale components, which are just a little larger than the cutoff scale, typically carry more energy. Hence, without explicit filtering which employs a filter coarser than the mesh size, the smallest resolved scales are by definition substantially affected by the employed numerical scheme. These scales however influence most strongly the contribution determined by the SGS model. In fact a complex discrete model for the SGS effect on the resolved flow is created which results from physical as well as numerical modelling. Consequently, the order of a method is not necessarily an appropriate notion in the context of LES. It rather has to be supplemented with a refined analysis like the modified wavenumber concept as e.g. discussed by Ferziger (1996). Let us illustrate these statements by means of Fig. 6.

Refering to eq. (5), the exact spatial derivative of $\overline{u}$ formulated in Fourier space is

$$\left(\widehat{\frac{\partial \overline{u}}{\partial x}}\right)(\omega) = i\omega\, \widehat{G}(\omega)\, \widehat{u}(\omega). \tag{28}$$

The numerical evaluation of $\partial\overline{u}/\partial x$ by a finite–difference formula corresponds to replacing the factor ω in (28) by a modified wavenumber $\omega_{eff}(\omega)$ which depends on the particular scheme employed. Derivation and formulas are given, e.g., by Ferziger & Peric (1996). For symmetric schemes this is a real quantity, otherwise it is complex. Starting from $\omega_{eff}(0) = 0$, $|\omega_{eff}|$ increases and then drops down to zero again. The point ω_Δ where this takes place is determined by the numerical grid employed; it is the highest frequency resolved by the grid. In a DNS this point would be pushed as far as possible to the right (Fig. 6a). The order of a discretization scheme can be reformulated in terms of the exponent p in $\lim_{\omega\to 0} |\omega - \omega_{eff}(\omega)| \propto \omega^p$. Obviously, the information about the order of a scheme is sufficient only if $\omega_\Delta \to \infty$ so that the solution to be computed is located entirely at $\omega/\omega_\Delta \approx 0$. If however ω_Δ approaches the relevant scales of the solution to be discretized, the behaviour of the whole curve ω_{eff} is decisive, not only the limit $\omega \to 0$. It is rather visible that computing a derivative with $\omega_{eff} \neq \omega$ amounts to replacing $\widehat{G}(\omega)$ in (28) by $\widehat{G}_{eff} = \omega_{eff}/\omega\ \widehat{G}(\omega)$. Hence the finite difference formula results in additional filtering applied to the derivative of $\overline{u}$ (Salvetti & Beux 1998). Fig. 6b furthermore shows that the decay of the error obtained with grid refinement in an LES depends on the behaviour of the solution itself, e.g. on the decay rate of its spectrum. This information is indispensable when aiming to assess the numerical error in an LES and to compare it with the size of the SGS term (Ghosal 1996).

So far we have discussed the discrete derivative operator which is a building block when discretizing the whole system of equations. Qualitatively, the real part of ω_{eff}/ω in the convection term introduces spurious or numerical dispersion while its imaginary part results in additional numerical dissipation. Analyzing the fully discrete system is much more complicated but can be achieved when disregarding boundary conditions etc. by the modified equation approach (Hirt 1968). This has been applied by Werner (1991) to a staggered finite volume discretization with Adams–Bashforth time scheme, central differences for the viscous term, and the QUICK convection scheme. Recall that the QUICK scheme (Leonard 1979) is a third order upwind interpolation scheme for the flux over the surface of a control volume. Werner observed that this combination results in a spurious 4th order dissipative term proportional to the cell Reynolds number $Re_{cell} = \overline{u}\Delta x/\nu$. The same analysis for a leap–frog time scheme with second order central differencing yields a 4th order error term which is independent of Re_{cell}. Such an analysis nicely shows that the upwind scheme produces excessive damping for large Re_{cell}. This, however, is precisely the working range of LES with typically $Re_{cell} = O(10000)$, even if ν is replaced by $\nu + \nu_t$. To demonstrate the effect in a real LES, Werner also computed a plane channel with $Re_\tau = 1954$ employing the Smagorinsky model. With a modified leap–frog scheme $\nu_t/\nu = 1.2$, $C = 0.14$, $Re_{cell} = 1350$ on the centerline. Analysis yields $|\nu_{num}/\nu| \approx 0.2$. With the QUICK upwind scheme the corresponding numbers are $\nu_t/\nu = 0.9$ and $|\nu_{num}/\nu| \approx 180$. Hence the numerical dissipation introduced by the upwinding exceeds the one by the SGS model by two orders of magnitude. Similar though mostly less detailed experiences have been reported in several papers by comparing the solution obtained with different schemes. The QUICK scheme and lower order upwind schemes gave worse results than a second order central scheme in LES of a circular cylinder (Breuer 1998). This was, though with decreasing impact, also observed for 5th and 7th

order upwinding (Beaudan & Moin 1994). Further studies of the numerical error in LES were performed by Vreman, Geurts & Kuerten (1994), Kravchenko & Moin (1997) and others. Hence, on the one hand upwind schemes can spoil the result by excessive damping. On the other hand, some researchers omit explicit SGS modelling and let the numerical dissipation of the employed scheme remove the energy. The MILES approach (Boris et al. 1992), e.g., falls into this class. Comte and Lesieur (1998) however found such schemes to be inferiour to explicit SGS modelling. In contrast to the numerical dissipation, the dispersion of a scheme is of lower importance as it has no effect on the energy drain which has been claimed to be the principal task of the SGS modelling. Dispersion, however, is related to the generation of spurious wiggles which in some LES of bluff bodies pose problems (Rodi et al. 1997).

4.3 Further developments

In order to improve the current status, attempts are made to separate more clearly the different ingredients in an LES. The aim is to study and improve each of them in a separate and controlled way. One of the directions pursued is explicit filtering as mentioned above. A similar approach is used by Vreman, Geurts & Kuerten (1994,1997) who use a value of $\overline{\Delta}$ larger than the mesh size of the grid, e.g. by a factor of two in the SGS model, which leads to increased SGS dissipation effectively damping the solution in a similar way as explicit filtering. A second direction is the use and improvement of higher order energy–conserving discretization schemes (Morinishi et al. 1998). They ensure that the total dissipation is entirely controlled by the SGS model and not by the discretization. Bearing in mind the uncertainty in SGS modelling, when for example determining the parameter C in the DSM, the practical importance of an energy–conserving scheme is presently not clear. A third direction is to use higher order methods as they narrow the range of scales which are influenced by the discretization of the filtered equations. Furthermore, filters recently have been devised so as to commute with discrete derivatives (Vasilyev, Lund & Moin 1998). This ideally ensures that apart from the SGS term τ_{ij} in eq. (8) no commutator term arises which would require modelling. Finally, "defiltering" has been applied to invert the attenuation of resolved scales by the implicit filtering related to the discretization (Stolz, Adams & Kleiser 1999). It uses an operation like multiplication of $\widehat{\overline{u}}(\omega)$ with $\widehat{G}(\omega)^{-1}$ to devise an estimate u^* for the true velocity u based on the resolved velocity $\overline{u}$, as may be illustrated with eq. (5) and Fig.4. This procedure requires higher order methods and principal adjustments such as restriction to certain scales since inverse filtering is ill–conditioned (imagine obtaining u from $\overline{u}$ in Fig.3a or 3b by backward diffusion). First results look promising.

5 Boundary conditions

We have mentioned already the mathematical problems when boundary conditions for filtered quantities have to be defined. From a physical point of view, the flow near a solid wall exhibits substantially different structures than away from it. In this region the "large scales" – in the sense that they significantly determine the overall properties – are of the order of the boundary layer thickness and hence typically much smaller than in the core of the flow, in particular if the Reynolds number is large. In addition, the small scales in this area exhibit substantial anisotropy and energy transfer mechanisms are different compared

to the core flow (Härtel 1996, Piomelli et al. 1996). This makes subgrid–scale modelling in the vicinity of walls a difficult task.

5.1 Resolution of the near–wall region

The most natural boundary condition at a wall is the no–slip condition. It requires however that the energy–carrying motion is resolved down to the wall. In an attached boundary layer this motion is mainly constituted by the well–known streaks of spanwise distance $\lambda_z \approx 100$ resolution of which requires $y^+ < 2$, $\Delta x^+ = 50 - 150$, $\Delta z^+ = 15 - 40$. (Piomelli & Chasnov 1996). The resulting simulation is in fact a hybrid one between an almost–DNS near the wall and an LES in the main part of the flow. If locally a fine grid is required an efficient discretization calls for a block–structured or an unstructured method. Care has to be taken however, since for example a low order FV method that locally splits each cell into a number of smaller ones introduces a sudden decrease in the size of the implicit filter by a factor of two at least in one direction. This may lead to problems with the SGS modelling. Kravchenko, Moin & Moser (1997) have developed a discretization that employs overlapping B–splines and hence results in a smoother transition of the effective resolution. It was successfully applied to channel flow up to $Re = 109410$. Another possibility is an unstructured finite element method as used by Rollet-Miet et al. (1999). Due to particular discretization issues discussed in this reference only very few codes of this kind are capable of LES up to now. With an unstructured code, one is still left with the task of generating a grid that fulfills the needs, in particular with respect to its influence on SGS modelling. Regardless which method is used to discretize and compute the near–wall region, the wall–resolving approach can result in substantial complexity and computational effort. Spalart et al. (1997) stressed that refinement needs to be performed not only in the wall–normal but also in the streamwise and spanwise directions and estimated that $O(10^{11})$ grid points would be necessary for a wing at $Re = 6.5 \cdot 10^6$ while "10^8 is impressive today". Also, resolving the flow in space is worthless if it is not also resolved properly in time, hence the CFL number has to be of order unity, a fact that even further increases the computational burden. To conclude: although a wall–resolving LES is appropriate for lower Re and transitional flows, a different approach is needed for higher Re, particularly when the interest of a simulation focuses on features away from the wall.

5.2 Wall functions

When for higher Re a wall–resolving LES is not possible, the way out is to use a near–wall model approximating the overall dynamic effects of the streaks on the larger outer scales which are resolvable by the LES. The most commonly used models are wall functions for bridging a region very close to the wall, often the viscous sublayer. Such wall functions are classically used in RANS methods, where they take the form:

$$\langle \tau_\omega \rangle = W(\langle u_1 \rangle, y_1) \tag{29}$$

Here, y_1 is the distance of the first grid point from the wall, $\langle \tau_\omega \rangle$ the average wall shear stress, $\langle u_1 \rangle$ the average tangential velocity at y_1, and W a functional dependence. Note that any relation $\langle u \rangle^+ = f(y^+)$ can be converted to the form (29). This can be the log–law, the 1/7–power law, a linear viscous law or even a numerical fit to DNS data. An appropriate blending is generally used so that W is defined from $y_1^+ \approx 0$ to y^+ of several hundreds.

Even if many physical properties such as the low–order moments and hence W are well–know for a certain flow – this is the case for the developed flow in a plane channel, for example – it is a delicate task to introduce this knowledge in the context of LES. The available information is of a statistical nature whereas the filtered velocity is an instantaneous, fluctuating quantity. On the other hand it has been demonstrated that the inner and outer regions of a turbulent boundary layer are only loosely coupled (Brooke & Hanratty (1993)) so that an artifical boundary condition bridging the inner layer has a chance to be successful (Piomelli 1998). One of these wall–function methods (Schumann 1975) employs the mean velocity $\langle\overline{u}(y_1)\rangle$, which is successively computed during the LES, to determine the average wall shear stress $\langle\tau_\omega\rangle$ from (29) with W being the logarithmic law of the wall. The same proportionality as between $\langle\overline{u}(y_1)\rangle$ and $\langle\tau_\omega\rangle$ is then assumed to hold also between the instantaneous quantities $\overline{u}(y_1)$ and τ_ω, in particular they are supposed to be in phase. This yields the instantaneous wall stress as

$$\tau_\omega = \frac{\langle\tau_\omega\rangle}{\langle\overline{u}(y_1)\rangle}\,\overline{u}(y_1) \tag{30}$$

which is used as a boundary condition in the LES. Werner & Wengle (1993) employed the 1/7–power law instead of the log law to avoid an iterative evaluation of W. Furthermore, they replaced (29) by $\tau_\omega = W(\overline{u}_1, y_1)$ so that the average velocity is no longer needed. Other combinations and variants are possible as well. A generalization of the approach for the subcritical flow around a cylinder is described by Fröhlich (2000). In the technically relevant case of a rough surface, using the wall–function approach is unavoidable since resolving the flow around each roughness element is impossible. The roughness effect is brought in by the roughness parameter in the log–law (Grötzbach 1977).

Wall function boundary conditions work reasonably well in simple flows and save substantial CPU time due to the reduced resolution requirements. They have also been applied to some complex flows around obstacles (Rodi et al. 1997) which, however, were found not to be very sensitive to variations in the boundary conditions.

5.3 Other approaches

Wall functions establish a relation between the local wall shear stress and the velocity at the wall–adjacent grid point. This can be generalized to the case where information on a line or a whole plane at some distance parallel to the wall is used to generate the wall–shear stress at a certain point. Such information can be introduced as a boundary condition in unsteady turbulent boundary layer equations which are solved along the wall within the wall cell using an embedded grid (Balaras, Benocci & Piomelli 1996) (cf. Fig. 7d). In these equations turbulence is modelled with an eddy viscosity depending on the wall distance. Similar work has been done by Cabot (1995,1996) where different models of this type were devised and applied to flow in a plane channel and over a backward facing step. Although yielding better results in some computations compared to wall functions, these methods have not found wide application yet due to their implementational complexity.

Another approach that can be introduced more easily in an LES is based on using the no–slip condition which in turn requires refinement in the wall–normal direction. Parallel to the wall, however, the step size of the outer region is maintained leading to substantial savings. The idea then is to replace the unresolved near–wall structures by elements from RANS simulations. Schumann (1975) decomposed τ_{ij} into an isotropic part for which the

Smagorinsky model is used and an anisotropic part resulting from the mean flow gradient. The latter part is modelled with an eddy viscosity $\nu_{t,an} = \min(c\Delta_{x,z}, \kappa d)d\langle\overline{u}\rangle/dy$ This is a RANS–like model in which close to the wall the size of the grid $\Delta_{x,z}$ is replaced by the distance from the wall d as a length scale. A similar switch is used in the DES approach of Spalart et al. (1997) mentioned above so that close to a wall the original RANS model is employed (see Fig. 7b). DES, although conceived for different applications, has been tested for channel flow by Nikitin et al. (2000). The authors observe a spurious buffer layer reflecting difficulties in connecting the quasi–steady RANS layer close to the wall to the outer unsteady computation. Further adjustments need to be introduced to apply DES in such cases. Bagett (1998) discussed the issue of blending RANS with LES turbulence models and points out the requirements for adequate spanwise resolution in the near–wall region in order to capture the energetically dominant features. If these are not captured, unphysical structures are generated which degrade the result.

5.4 Inflow and outflow conditions

After discussing the boundary conditions at solid walls we briefly mention the conditions at artificial boundaries, an issue shared with DNS. Turbulent outflow boundaries are relatively uncritical. Here, damping zones or convective conditions are generally applied which allow vortices to leave the computational domain with only small perturbations of the flow in its interior. A convective condition for a quantity ϕ reads

$$\frac{\partial\phi}{\partial t} + U_{conv}\frac{\partial\phi}{\partial n} = 0 \tag{31}$$

applied on the outlet boundary with n the outward normal coordinate and U_{conv} an appropriate convection velocity such as the bulk velocity.

The difficulty posed by turbulent inflow conditions stems from the fact that LES computes a substantial part of the spectrum and hence requires specification of the inflow conditions in all this spectral range, not just the mean flow. The need for this information can be avoided by imposing streamwise periodicity with a sufficient periodic length, but this is inapplicable in many practical flows. Imposing the mean flow plus random perturbations is generally not successful since these perturbations are unphysical so that a large upstream distance must be computed to produce the correct turbulence statistics. With more sophisticated perturbations the distance can be shortened. This is a subject of current research. If feasible the best solution is to impose some fully developed flow at the inlet. A separate companion LES, e.g. with streamwise periodicity, can then be performed to generate velocity signals at the grid points in the inflow plane of the main LES. An example is the flow around a single cube investigated in Rodi et al. (1997).

5.5 Sample computations

In order to illustrate the above discussion, we present results from a standard test case for LES calculations, namely fully developed plane channel flow. For this flow between two infinitely extended plates, periodic conditions can be imposed in the streamwise direction x and the spanwise direction z, with typical domain sizes of $L_x = 2\pi$ and $L_z = \pi$, respectively. Reference quantities are the channel half–width δ and the bulk velocity U_b. DNS of this flow has been performed for low and medium Reynolds number of which the currently

highest is $Re_b = U_b\delta/\nu = 10935$ (Moser, Kim & Mansour 1999) employing a high–precision spectral method with $384 \times 257 \times 384$ points. This Reynolds number has been used in the computations below. The results have been obtained with the structured collocated finite volume code LESOCC developed by Breuer & Rodi (1994). The dynamic Smagorinsky model was used with test–filtering and averaging in planes parallel to the walls. The bulk Reynolds number was fixed and an external pressure gradient adjusted so as to yield the desired flow rate.

Fig.8 shows a computation where resolving the near–wall flow has been attempted, i.e. no wall–function was used. The number of points in the y direction is 65 and a stretching of 11% has been applied to cluster them close to the walls. The figure shows the average streamwise velocity and the rms–fluctuations. The computed shear stress τ_w yields $Re_\tau = 504$ which is much below the $Re_\tau = 590$ in the DNS. The value of $u_\tau = \sqrt{\tau_w/\rho}$ determines the scaling of the axes, and in particular the $\langle\overline{u}\rangle^+ = f(y^+)$–curve is quite sensitive to it. If the v– and w– fluctuations are plotted in outer scaling, i.e. not by u_τ, they are even further below the DNS curves. The observed failure occurs because resolving the flow near the wall requires adequate discretization in all three directions, not just normal to the wall. Here in particular the spanwise resolution is too coarse. In Fig.9 the wall–normal resolution has been improved using 159 points in y with clustering in the buffer layer accompanied by a substantially better resolution in spanwise direction. The computed shear stress yields $Re_\tau = 598.5$ and the Reynolds stresses compare quite satisfactorily with the DNS data. It is obvious that with a structured discretization the grid in the interiour of the channel is finer than it really needs to be, due to the requirements near the wall. To avoid this, a method with local refinement is beneficial as discussed above. Fig. 10 presents a computation using the wall function of Schumann (1975). In the wall–normal direction 39 equidistant volumes are used. In this case the first cell center is still located in the buffer layer, but the viscous sublayer is well bridged. The computed wall shear stress gives $Re_\tau = 589.5$ which compares very well with $Re_\tau = 590$ in the DNS. The Reynolds stresses are well predicted, the v–fluctuations being somewhat too small. With this approach it is of course not possible to reproduce the peak in the u–fluctuations close to the wall. For an LES using a wall function the present Reynolds number is relatively low. With higher Re the first point usually lies beyond the buffer layer at $y^+ \approx 100$.

In Fig. 11 we finally show cuts of the instantaneous u– and w–velocity of the third case. Straight lines have been inserted connecting the data points. The angles they form show that, as discussed in Section 4, on the grid level the discrete solution is not smooth, i.e. the velocity scales close to the cutoff are hardly resolved. Hence, any gradient computed from these values by, e.g., a second order scheme can only be a crude approximation to the "true" gradient. Recall that gradients enter in the contribution of the SGS model. This figure illustrates the close interplay between the numerical discretization and the subgrid–scale modelling. The amount of SGS dissipation in eddy–viscosity models can be monitored by the ratio ν_t/ν. It varies locally and in the above computations attains values up to 7 in the last case which shows the dominance of the SGS dissipation with respect to the resolved dissipation. Further applications of LES, in particular to bluff body flows, are discussed in other chapters of this volume.

6 Concluding remarks

We have described the kconcept of the Large–Eddy Simulation technique which in fact is extremely simple and makes it appealing. It turns out, however, that several issues are not simple for numerical or physical reasons. We have aimed at making the reader aware of these points and at clarifying related concepts. In practice, LES is characterized by a large number of decisions concerning the numerical and physical modelling which have to be taken and which all influence the final result. Thorough testing is still a major occupation of the community, and this will presumably not change in the near future.

On the other hand, LES has a potential on several levels. The first is the determination of statistical quantities such as the average flow field with a higher accuracy than obtained by statistical models. This is based on interchanging the order "first averaging – then computing" (RANS) to "first computing – then averaging" (LES). To pay off, the drastic increase in cost has to be justified by an improved quality of the results. The next level is the determination of statistical quantities which are inaccessible to RANS such as two–point correlations. The third level is to use the instantaneous information on the structure of the flow in order to improve the understanding of vortex dynamics, transition phenomena, etc. or to determine dynamic loading. Finally, this information can be coupled to other physical processes either within the flow field such as the generation of sound, the transport of scalars (temperature, sediment, ...), chemical reactions, etc., or to external processes such as the dynamical response of a solid structure. This type of feature is required for important fields of research such as fluid–structure aerodynamic coupling and turbulence control. In the future, the applications of LES will turn from the present academic cases to more applied configurations.

References

J.S. Baggett. On the feasibility of merging LES with RANS for the near–wall region of attached turbulent flows. In *Annual Research Briefs 1998*, pages 267–277. Center for Turbulence Research, 1998.

E. Balaras, C. Benocci, and U. Piomelli. Two-layer approximate boundary conditions for large–eddy simulations. *AIAA Journal*, 34:1111–1119, 1996.

P. Beaudan and P. Moin. Numerical experiments on the flow past a circular cylinder at sub–critical Reynolds number. Technical Report TF-62, Stanford University, 1994.

J.P. Boris, F.F. Grinstein, E.S. Oran, and R.L. Kolbe. New insights into large eddy simulation. *Fluid Dyn. Res.*, 10:199, 1992.

M. Breuer. Large eddy simulations for the flow past a circular cylinder, numerical and modelling aspects. *Int. J. Numerical Methods in Fluids*, 28, 1998.

M. Breuer and W. Rodi. Large eddy simulation of turbulent flow through a straight square duct and a 180^o bend. In P.R. Voke, R. Kleiser, and J.P. Chollet, editors, *Fluid Mech. and its Appl.*, volume 26. Kluwer Academic, 1994.

J.W. Brooke and T. J. Hanratty. Origin of turbulence-producing eddies in a channel flow. *Phys. Fluids*, 5:1011–1022, 1993.

W. Cabot. Large–eddy simulations with wall models. In *Annual Research Briefs 1995*, pages 41–50. Center for Turbulence Research, 1995.

W. Cabot. Near–wall models in large eddy simulations of flow behind a backward facing step. In *Annual Research Briefs 1996*, pages 199–210. Center for Turbulence Research, 1996.

J.P. Chollet and M. Lesieur. Parameterization of small scales of three dimensional isotropic turbulence. *J. Atmos. Sci.*, 38:2747–2757, 1981.

P. Comte and Marcel Lesieur. Large eddy simulation of compressible turbulence. In *Advances in Turbulence Modelling*, number 1998–05 in Lecture Series. Von Karman Institute for Fluid Dynamics, Rhode Saint Genèse, Belgium, 1998.

L. Davidson. Large Eddy Simulation: A dynamic one–equation subgrid model for three–dimensional recirculating flow. In *11th Symp. on Turbulent Shear Flows*, volume 3, pages 26.1–26.6, Grenoble, 1997.

J. Ferziger and M. Peric. *Computational Methods for Fluid Dynamics*. Springer Verlag, 1996.

J.H. Ferziger. Large eddy simulation. In T.B. Gatski, M.Y. Hussaini, and J.L. Lumley, editors, *Simulation and modelling of turbulent flows*, ICASE/LaRC Series in Comp. Sci. and Eng., pages 109–154. Oxford University Press, New York, 1996.

J. Fröhlich. LES of vortex shedding past circular cylinders. to appear in Proceedings of ECCOMAS 2000, Barcelona, 11–14 September, 2000.

J. Fröhlich, W. Rodi, Ph. Kessler, S. Parpais, J.P. Bertoglio, and D. Laurence. Large eddy simulation of flow around circular cylinders on structured and unstructured grids. In E.H. Hirschel, editor, *Notes on Numerical Fluid Mechanics*, volume 66, pages 319–338. Vieweg, 1998.

J. Fröhlich, W. Rodi, J.P. Bertoglio, U. Bieder and H. Touil. Large eddy simulation of flow around circular cylinders on structured and unstructured grids, II. In E.H. Hirschel, editor, *Notes on Numerical Fluid Mechanics*, to appear.

C. Fureby, G. Tabor, H.G. Weller, and A.D. Gosman. Differential subgrid stress models in large eddy simulations. *Phys. Fluids*, 9:3578–3580, 1997.

M. Germano. Turbulence: the filtering approach. *J. Fluid Mech.*, 238:325–336, 1992.

M. Germano. From RANS to DNS: Towards a bridging model. In P.R. Voke, N.D. Sandham, and L. Kleiser, editors, *Direct and Large–Eddy Simulation III*, volume 7 of *ERCOFTAC Series*, pages 225–236. Kluwer Academic, 1999.

M. Germano, U. Piomelli, P. Moin, and W.H. Cabot. A dynamic subgrid–scale eddy viscosity model. *Phys. Fluids A*, 3:1760–1765, 1991.

B. J. Geurts. Balancing errors in large–eddy simulation. In P.R. Voke, N.D. Sandham, and L. Kleiser, editors, *Direct and Large–Eddy Simulation III*, volume 7 of *ERCOFTAC Series*, pages 1–12. Kluwer Academic, 1999.

S. Ghosal. An analysis of numerical errors in large–eddy simulations of turbulence. *J. Comput. Phys.*, 125:187–206, 1996.

G. Grötzbach. Direct numerical simulation of secondary currents in turbulent channel flow. In H. Fiedler, editor, *Lecture Notes in Physics*, volume 76, pages 308–319. Springer–Verlag, 1977.

C. Härtel. Turbulent flows: direct numerical simulation and large–eddy simulation. In R. Peyret, editor, *Handbook of Computational Fluid Mechanics*, pages 283–338. Academic Press, 1996.

C. W. Hirt. Heuristic stability theory for finite–difference equations. *J. Comp. Phys.*, 2:339–355, 1968.

K. Horiuti. A new dynamic two–parameter mixed model for large-eddy simulation. *Phys. Fluids*, 9:3443–3464, 1997.

A. G. Kravchenko and P. Moin. On the effect of numerical errors in large eddy simulation of turbulent flows. *J. Comp. Phys.*, 131:310–322, 1997.

A.G. Kravchenko, P. Moin, and R. Moser. Zonal embedded grids for numerical simulations of wall–bounded turbulent flows. *J. Comp. Phys.*, 127:412–423, 1997.

A. Leonard. Energy cascade in large eddy simulations of turbulent fluid flows. *Adv. Geophys.*, 18A:237, 1974.

M. Lesieur. *Turbulence in Fluids*, volume 1 of *Fluid mechanics and its applications*. Kluwer Academic Publisher, P.O. Box 322,3300 AH Dordrecht, The Netherlands, 3 edition, 1997.

M. Lesieur and O. Métais. New trends in large–eddy simulations of turbulence. *Ann. Rev. Fluid. Mech.*, 28:45–82, 1996.

D.K. Lilly. A proposed modification of the Germano subgrid-scale closure method. *Phys. Fluids A*, 4:633–635, 1991.

S. Liu, C. Meneveau, and J. Katz. On the properties of similarity subgrid–scale models as deduced from measurements in a turbulent jet. *J. Fluid Mech.*, 275:83–119, 1994.

T.S. Lund and H.-J. Kaltenbach. Experiments with explicit filtering for LES using a finite–difference method. In *Annual Research Briefs 1995*, pages 91–105. Center for Turbulent Research, 1995.

M. Meinke, Th. Rister, F. Rütten, and A. Schvorak. Simulation of internal and free turbulent flows. In H.-J. Bungartz, F. Durst, and C. Zenger, editors, *High Performance Scientific and Engineering Computing*. Springer, 1998.

O. Métais and M. Lesieur. Spectral large–eddy simulation of isotropic and stable–stratified turbulence. *J. Fluid Mech.*, 239:157–194, 1992.

P. Moin. Numerical and physical issues in large eddy simulation of turbulent flows. In *Proceedings of the International Conference on Fluid Engineering, Tokyo, July 13-16, 1997*, volume 1, pages 91–100. Japan Society of Mechanical Engineers, 1997.

R.D. Moser, J. Kim, and N.N. Mansour. Direct numerical simulation of turbulent channel flow up to $Re_\tau = 590$. *Phys. Fluids*, 11:943–946, 1999.

N.V. Nikitin, F. Nicoud, B. Wasisto, K.D. Squires, and P.R. Spalart. An approach to wall modelling in large–eddy simulations. submitted, 2000.

U. Piomelli. Large eddy simulation turbulent flows. In *Advances in Turbulence Modelling*, number 1998–05 in Lecture Series. Von Karman Institute for Fluid Dynamics, Rhode Saint Genèse, Belgium, 1998.

U. Piomelli, W.H. Cabot, P. Moin, and S. Lee. Subgrid–scale backscatter in turbulent and transitional flows. *Phys. Fluids A*, 3:1766–1771, 1991.

U. Piomelli and J. Liu. Large eddy simulation of rotating channel flows using a localized dynamic model. *Phys. Fluids*, 7:839–848, 1995.

U. Piomelli, P. Moin, and J. H. Ferziger. Model consistency in large eddy simulation of turbulent channel flows. *Phys. Fluids*, 31:1884–1891, 1988.

U. Piomelli, Y. Yu, and R. J. Adrian. Subgrid–scale energy transfer and near–wall turbulence structure. *Phys. Fluids*, 8:215–224, 1996.

W. C. Reynolds. The potential and limitations of direct and large eddy simulations. In J.L. Lumley, editor, *Lecture Notes in Physics*, volume 357, pages 313–343. Cornell University Ithaca, Springer–Verlag, 1989.

W. Rodi, J.H. Ferziger, M. Breuer, and M. Pourquié. Status of large eddy simulation: Results of a workshop. *J. Fluid Eng.*, 119:248–262, 1997.

P. Rollet-Miet, D. Laurence, and J.H. Ferziger. LES and RANS of turbulent flow in tube bundles. *Int. J. Heat Fluid Flow*, 20:241–254, 1999.

M. V. Salvetti and S. Banerjee. A priori tests of a new dynamic subgrid–scale model for finite–difference large–eddy simulations. *Phys. Fluids*, 7:2831, 1995.

M.V. Salvetti and F. Beux. The effect of the numerical scheme on the subgrid scale term in large-eddy simulation. *Physics of Fluids*, 10:3020–3022, 1998.

U. Schumann. Subgrid scale model for finite difference simulations of turbulent flows in plane channels and annuli. *J. Comput. Phys.*, 18:376–404, 1975.

J.S. Smagorinsky. General circulation experiments with the primitive equations, I, the basic experiment. *Mon. Weather Rev.*, 91:99–164, 1963.

P.R. Spalart and S.R. Allmaras. A one–equation turbulence model for aerodynamic flows. *La Recherche Aérospatiale*, 1994.

P.R. Spalart, W.-H. Jou, M. Strelets, and S.R. Allmaras. Comments on the feasibility of LES for wings, and on a hybrid RANS/LES approach. In C. Liu and Z. Liu, editors, *Advances in DNS/LES*. Greyden Press, 1997.

C. G. Speziale. A combined large–eddy simulation and time–dependent rans capability for high–speed compressible flows. *J. Sci. Comput.*, 13:253–274, 1998.

S. Stolz, N.A. Adams, and L. Kleiser. The approximate deconvolution procedure applied to turbulent channel flow. In P. Voke, N.D. Sandham, and L. Kleiser, editors, *Direct and Large–Eddy Simulation III*. Kluwer Academic, 1999.

T. Tamura, I. Ohta, and K Kuwahara. On the reliability of two–dimensional simulation for unsteady flows around a cylider–type. *J. of Wind Eng. and Indust. Aerodyn.*, 35:275–298, 1990.

H. Tennekes and J.L. Lumley. *A first course in turbulence*. MIT Press, 1972.

U.Piomelli and J.R. Chasnov. Large–Eddy Simulations: theory and applications. In M. Hallbäck et al., editor, *Turbulence and Transition Modelling*, pages 269–331. Kluwer Academic, 1996.

O.V. Vasilyev, T.S. Lund, and P. Moin. A general class of commutative filters for LES in complex geometries. *J. Comput. Phys.*, 146:82–104, 1998.

B. Vreman, B. Geurts, and H. Kuerten. Discretization error dominance over subgrid terms in Large Eddy Simulation of compressible shear layers in 2d. *Communications in Numerical Methods in Engineering*, 10:785–790, 1994.

B. Vreman, B. Geurts, and H. Kuerten. On the formulation of the dynamic mixed subgrid–scale model. *Phys. Fluids*, 6:4057–4059, 1994.

B. Vreman, B. Geurts, and H. Kuerten. Large–Eddy simulation of the turbulent mixing layer. *J. Fluid Mech.*, 339:357–390, 1997.

H. Werner. *Grobstruktursimulation der turbulenten Strömung über eine querliegende Rippe in einem Plattenkanal bei hoher Reynoldszahl*. PhD thesis, Technische Universität München, 1991.

H. Werner and H. Wengle. Large–Eddy Simulation of turbulent flow over and around a cube in a plane channel. In U. Schumann et al., editor, *8th Symp. on Turb. Shear Flows*, 1993.

Y. Zang, R.L. Street, and J.R. Koseff. A dynamic mixed subgrid–scale model and its application to turbulent recirculating flows. *Phys. Fluids*, 5(12):3186–3196, 1993.

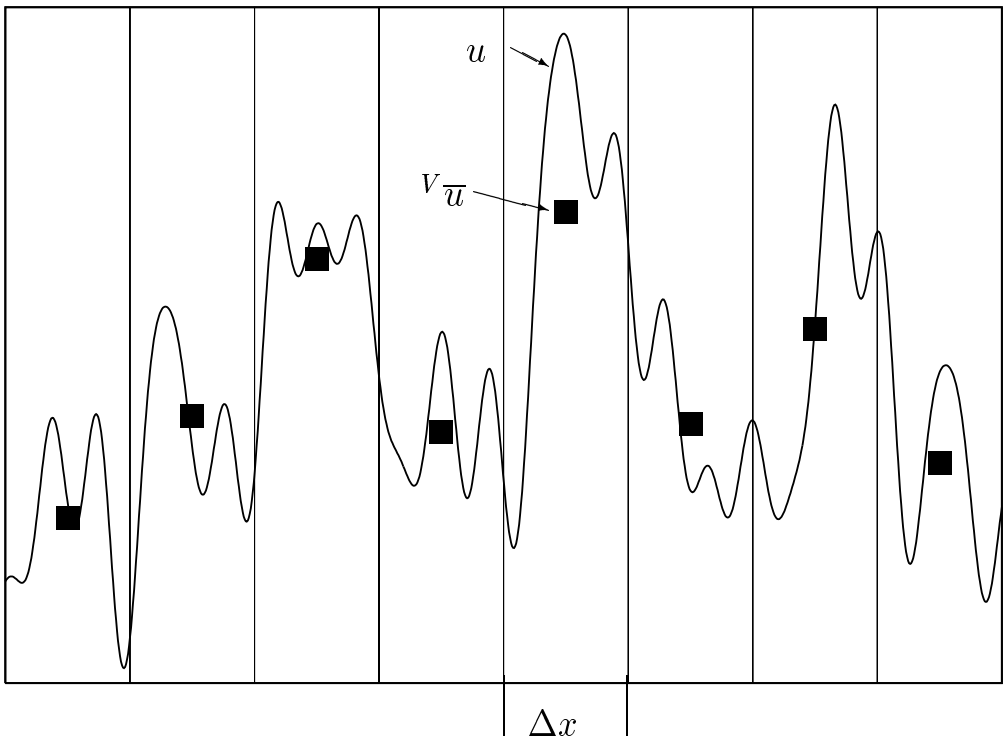

Figure 1: Illustration of Schumann's approach to LES as discussed in the text.

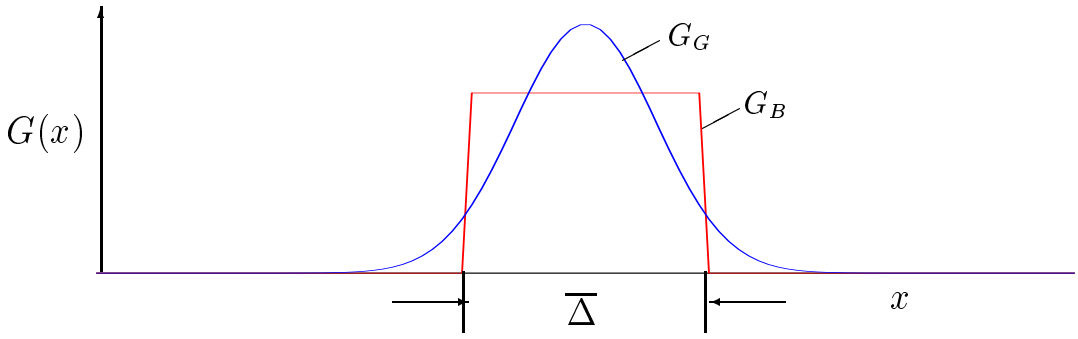

Figure 2: Gaussian filter G_G and box filter G_B as defined in the text, both plotted for the same filter width $\overline{\Delta}$.

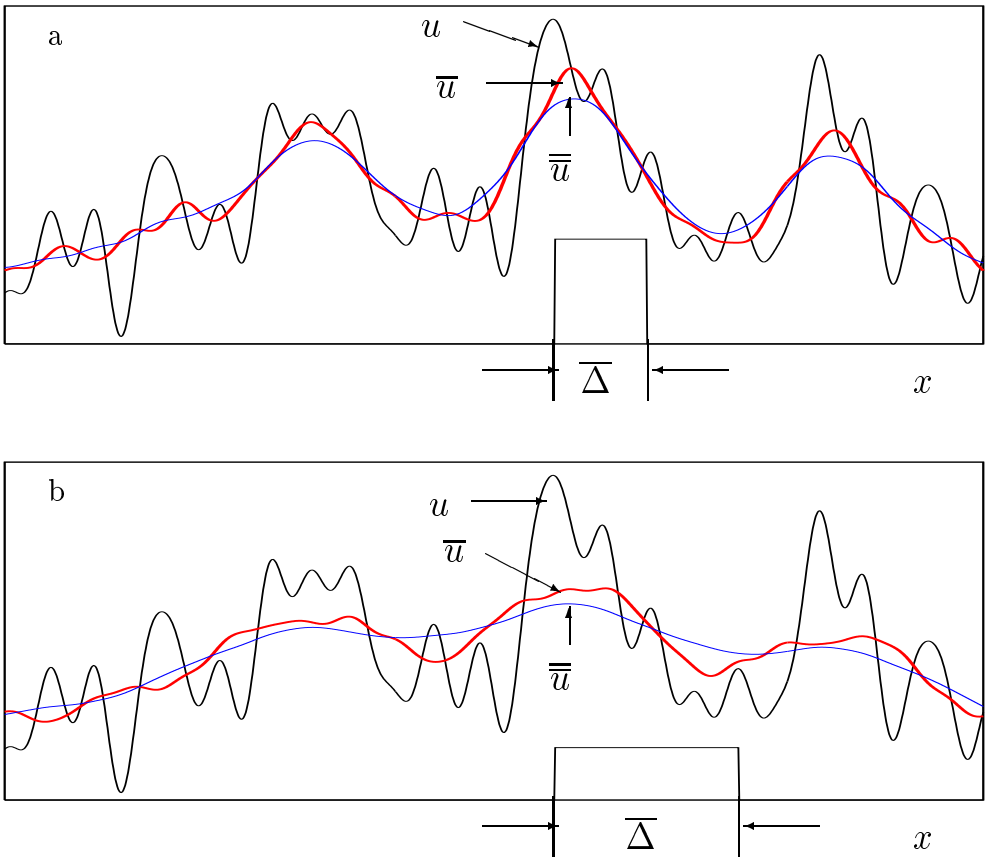

Figure 3: Filtered functions $\overline{u}$ and $\overline{\overline{u}}$ obtained from $u(x)$ by applying a box filter, a) narrow filter, b) wide filter,

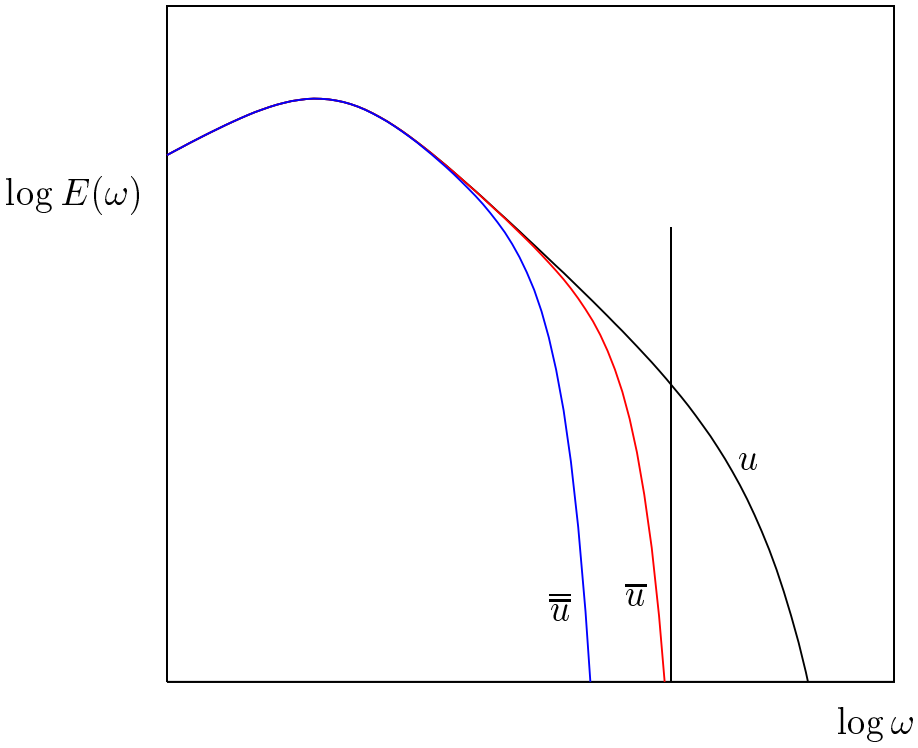

Figure 4: Effect of filtering on the spectrum. Here the box filter is used corresponding to Figure 3, but the curves are similar for other filters such as the Gauss Filter. u' and $\overline{u'}$ are illustrated by the area between the curves for u and $\overline{u}$, and $\overline{u}$ and $\overline{\overline{u}}$, respectively. The vertical line is related to the Fourier cutoff filter on the same grid.

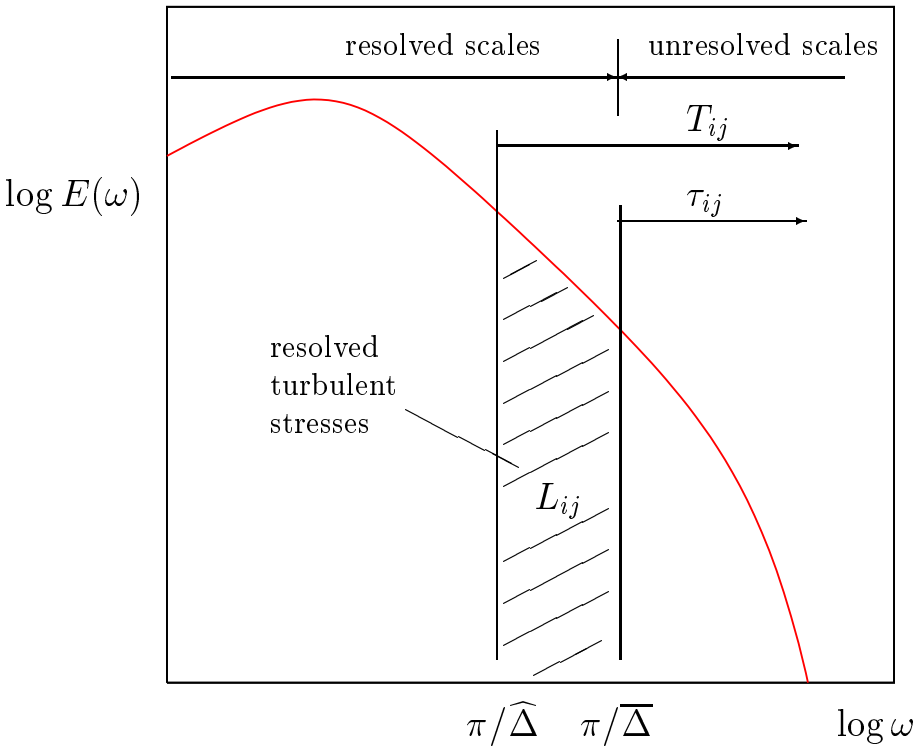

Figure 5: Illustration of the dynamic modelling idea as discussed in the text.

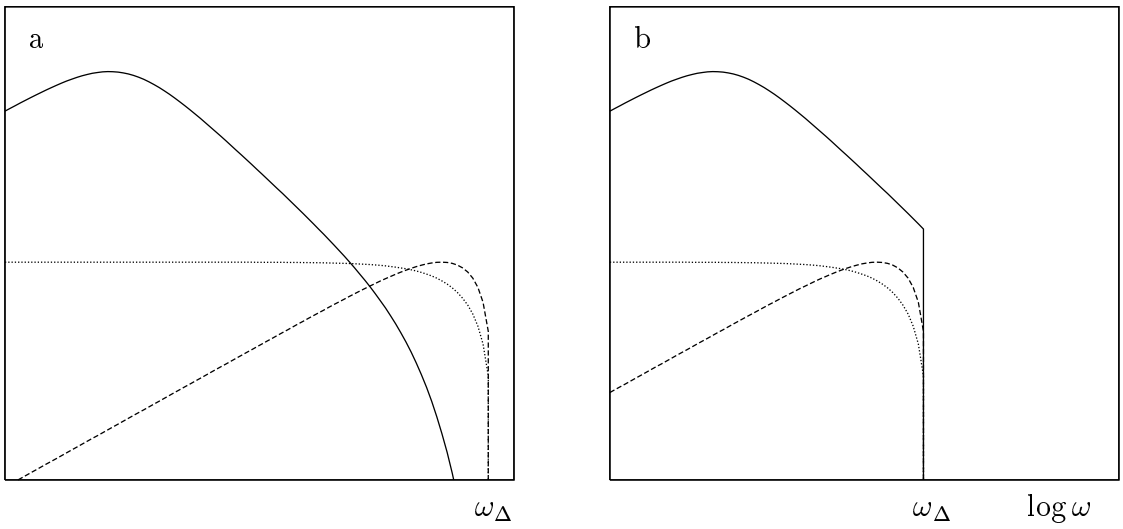

Figure 6: Discetization of derivatives (Sketch) in case of a DNS (a) and an LES (b); —– spectrum of u or $\overline{u}$, - - - $\omega_{eff}, \cdots \omega_{eff}/\omega$, the additional filter when numerically computing a derivative as discussed in the text, here for a second–order central formula. The vertical axis has an arbitrary scale. In the LES case we consider $\overline{u}$ to be obtained by an ideal low pass filter for illustration. Observe that due to the logarithmic frequency scale 88 % of the discretization points correspond to the range between the maximum of ω_{eff} and ω_Δ for a second order scheme in a three dimensional computation.

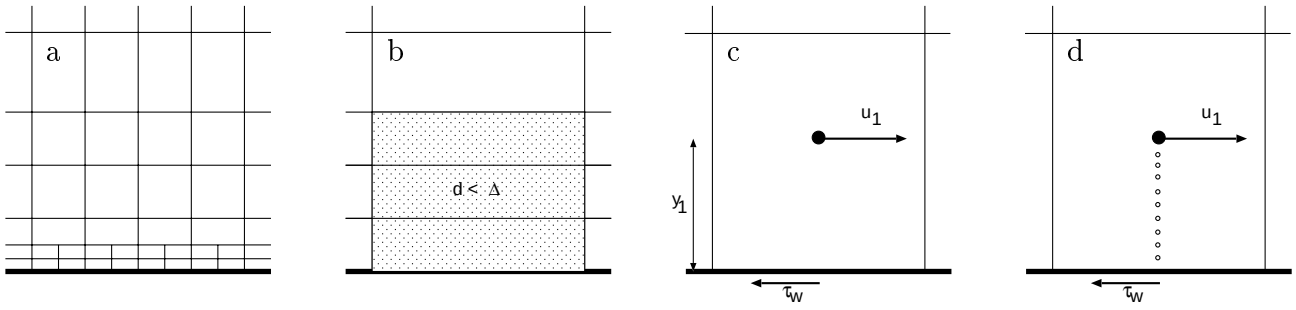

Figure 7: Schematical pictures for the different approaches close to solid walls: a) resolving the near–wall structure, b) blending with a RANS model, c) application of a wall function, d) determination of wall stress by boundary layer equation solved along the wall on an imbedded grid.

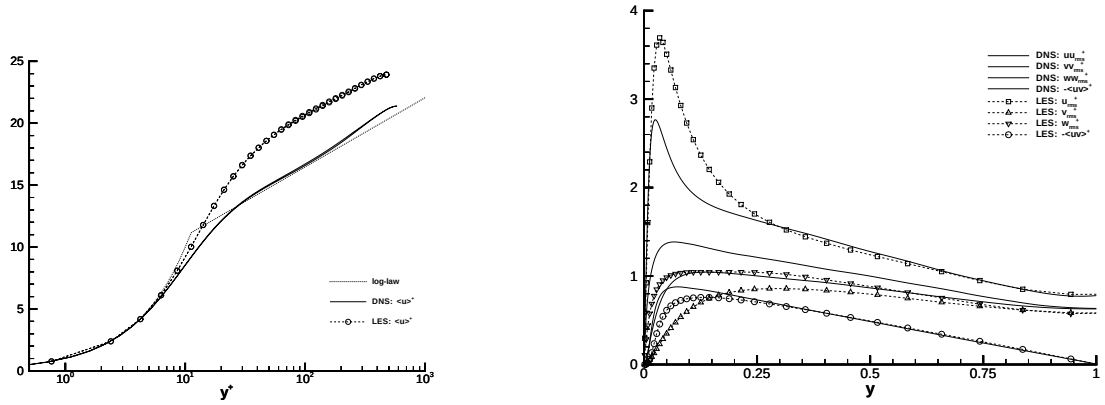

Figure 8: Computation without wall function using $\Delta x^+ = 62, \Delta z^+ = 30, \Delta y_1^+ = 1.8$. Left: u^+, right: $u^+_{rms}, v^+_{rms}, w^+_{rms}, -\langle uv \rangle^+$. Continuous lines are DNS data, symbols LES.

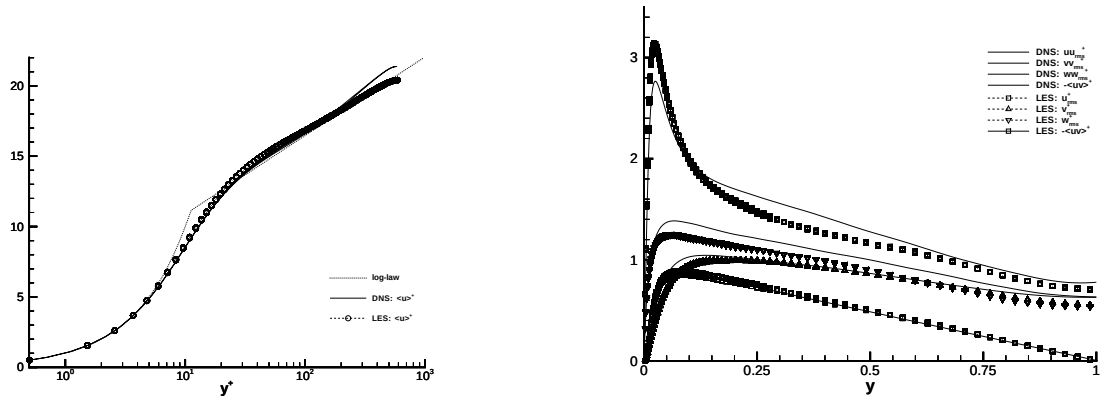

Figure 9: Computation without wall function using $\Delta x^+ = 50, \Delta z^+ = 16, \Delta y_1^+ = 1$. Labels as in Fig. 8.

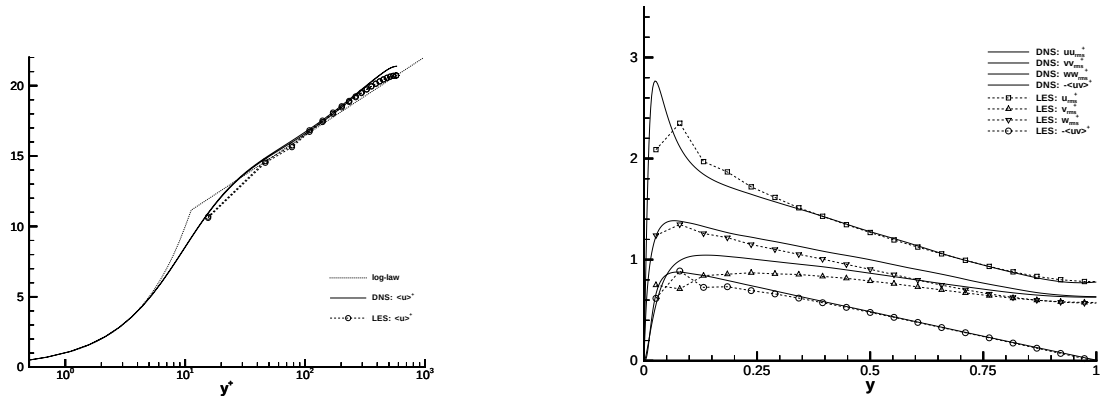

Figure 10: Wall function computation with $\Delta x^+ = 62, \Delta z^+ = 30, \Delta y_1^+ = 31$. Labels as in Fig. 8.

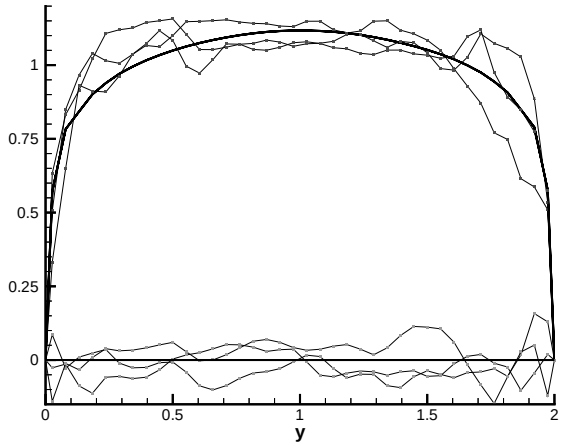

Figure 11: Velocities $\overline{u}$ (upper curves) and $\overline{w}$ (lower curves) at three arbitrary cuts $x = const.$, $z = const.$ in the computation of Fig.10. Thin lines connect the instantaneous values, thick lines show the corresponding averages.